Response of a Thin Flat Scored Metallic Disc Under Pressure Impulse

K. Gopinath,[$] V. Narayanamurthy[#,*] and Y.V.D. Rao[$]

[$]*Department of Mechanical Engineering, BITS Pilani-Hyderabad, India- 500 078*
[#]*Directorate of Systems Integration, Research Centre Imarat, Hyderabad, India - 500 069.*
[*]*Email: v.narayanamurthy@rcilab.in*

ABSTRACT

This paper presents the large deformation, and failure response of a thin flat scored metallic disc (FSMD) subjected to a pressure impulse as experienced in a break-away disc or an explosion vent. The response of this thin FSMD is numerically simulated for a loading rate and validated with an experiment, where a good agreement is found on plastic strains, burst pressure, and deformation pattern. The loading rate and several geometric parameters of FSMD significantly influence its response. Therefore, the influence of loading rate ($\dot{P}$), score depth and width-to-disc thickness ratio (t_1/t and b/t), diameter-to-disc thickness ratio (D/t), score length-to-disc radius ratio (l/R), score pattern, and score geometry on the deformation and failure response of the thin FSMD is thoroughly investigated. The studies demonstrate that 1) the failure initiation point shifts from disc centre to between 1/5th and 1/3rd radius for loading rates $\leq$ 25 MPa/s; 2) the responses such as burst pressure, burst time, central deflection, and equivalent strain are i) sensitive to the loading rates up to 100 MPa/s, ii) sensitive to score's depth, only up to 0.6t and insensitive to score's width, iii) significantly unaffected for the number of scores $N > 8$, iv) stabilised for $l/R > 0.5$ and $D/t >$ 250, v) almost the same for semi-circular, rectangular and triangular score geometries, and vi) very minimal for the number of scores $N = 3$; and 3) the failure do not initiate and propagate along all scores for $N > 4$ in the disc.

Keywords: Flat scored metallic disc; Score geometry; Score pattern; Large deformation; Failure; Impulsive load; Explicit finite element analysis

NOMENCLATURE

A	Yield stress (MPa)
B	Strain hardening coefficient (MPa)
b	Score/groove width (mm)
C	Strain rate coefficient
D_1, D_2, D_3, D_4, D_5	Johnson-Cook damage parameters
E	Young's modulus (MPa)
m	Thermal softening exponent
N	Number of scores/grooves
n	Strain hardening exponent
P	Pressure (MPa)
$\dot{P}$	Loading rate (MPa/s)
P_b	Burst pressure (MPa)
r	Radius of the disc (mm)
R	Maximum radius of the disc (mm)
t	Rupture disc sheet thickness (mm)
t_1	Score/groove depth (mm)
t_b	Burst time, i.e., time taken for burst (s)
u_x, u_y, u_z	Displacements in x,y, and z directions, respectively (mm)
w_{max}	Central deflection, i.e., maximum deflection at disc centre (mm)
ε	Plastic strain
ε_{max}	Maximum equivalent plastic strain
ε_{xx}	Strain in the x-direction
ε_{yy}	Strain in the y-direction
ε_{eq}	Equivalent plastic strain
$\dot{\varepsilon}$	Strain rate (1/s)
$\dot{\varepsilon}_{max}$	Maximum strain rate (1/s)
μ	Poison's ratio
ρ	Density of material (kg/m³)
σ_{eq}	Equivalent stress i.e. von-Mises stress (MPa)
σ_{max}	Maximum equivalent stress (MPa)

1. INTRODUCTION

Thin Flat Scored Metallic Disc (FSMD) finds application as a burst disc or an explosion vent designed to fail at a given pressure impulse. It is used as a sacrificial element in pneumatic or hydraulic systems to protect the equipment from high surge pressures[1]. It is also used as a burst disc in the shock tube apparatus between high and low-pressure chambers[2]. In blast and explosive applications, it is known as an explosion vent, rupture panel, or rupture disc and is used to protect large

equipment or buildings during an internal explosion or blast. This high loading rate application can be extended to rocket silos where it can be used generally as a protective cover but can be opened without manual intervention upon generation of a pressure impulse.

Flat thin metallic discs are commonly used in low-pressure applications similar to pressure relief valves. Their burst pressures are always not constant and repeatable due to the absence of any predefined scores or notches. Therefore, thin FSMDs are always preferred to (a) induce stress-triaxiality and initiate the failure in a preferred pattern along the scores, and (b) provide a nearly constant burst pressure. They undergo large inelastic deformation and rupture under higher loading rates and have been studied extensively under air blast and explosive loadings[3-18]. A comprehensive review by Nurick et al.[3,4] in 1989 compares the theoretical and experimental results of fully clamped flat circular plates subjected to impulsive load. The research between 1989 and 2016 on thin plates subjected to impulsive load was reviewed by Yuen et al.[5] in 2017, and they summarised the advancements in predicting the central deflection. Close agreement between theory and experiment is reported even after neglecting the effects of strain hardening and strain rate sensitivity. Failures in unscored metallic discs are observed in three different modes, namely, failure mode-I in which the disc exhibits a large plastic deformation under low impulse levels, failure mode-II in which a tensile failure is observed at the boundary or central area of the disc when the impulse increases to a threshold limit, and failure mode-III in which transverse shear occurs at the boundary of the disc upon a further increase in the impulsive load. Yuan et al.[16] shown that an increase in the blast duration delays the transition between various deformation modes. Even the boundary conditions influence the tear and shear failures of plates. Edge sharpness at fixed boundary accelerates initiation of failure at the boundary[8-11].

Usually, the burst discs are circular and featured to clamp between two flanges. They are classified as solid, scored, and composite with slit and tabs. A burst disc with scores featured on one side is shown in Fig. 1, where the scores help i) to reduce the burst pressure, ii) in making the disc from a thicker sheet to facilitate manufacturing, and iii) to ensure failure with definite rupture pattern through the formation of petals and thereby avoiding fragmentation[1]. Jeong et al.[19] simulated the effect of groove thickness on the burst pressure of forward domed disc. Colombo et al.[20] experimented with the failure of a flat plate with rectangular scores with cross configuration under uniform pressure and concluded that a minimum score depth-to-plate thickness ratio of 0.4 is essential for failure initiation in scores. Standards and codes[21] provide general guidelines for selecting burst discs used as safety pressure relief valves. Still, they are not applicable for discs, i.e., rupture panels subjected to impulsive and higher loading rates. The design guidelines and extensive studies on the failure of FSMD are unavailable in the literature. The response of this thin FSMD is influenced by its several geometric parameters and loading rate.

Therefore, an attempt is made in this paper to understand the behaviour of clamped, thin FSMD subjected to an impulsive air blast. The response is numerically simulated for a loading rate and validated with experiments and subsequently, the influence of loading rates ($\dot{P}$), score depth and width-to-disc thickness ratio (t_l/t and b/t), diameter-to-disc thickness ratio (D/t), score length-to-disc radius ratio (l/R), score pattern (i.e., number of scores N), and score geometry on the deformation and failure response of the thin FSMD is thoroughly investigated and discussed in this paper.
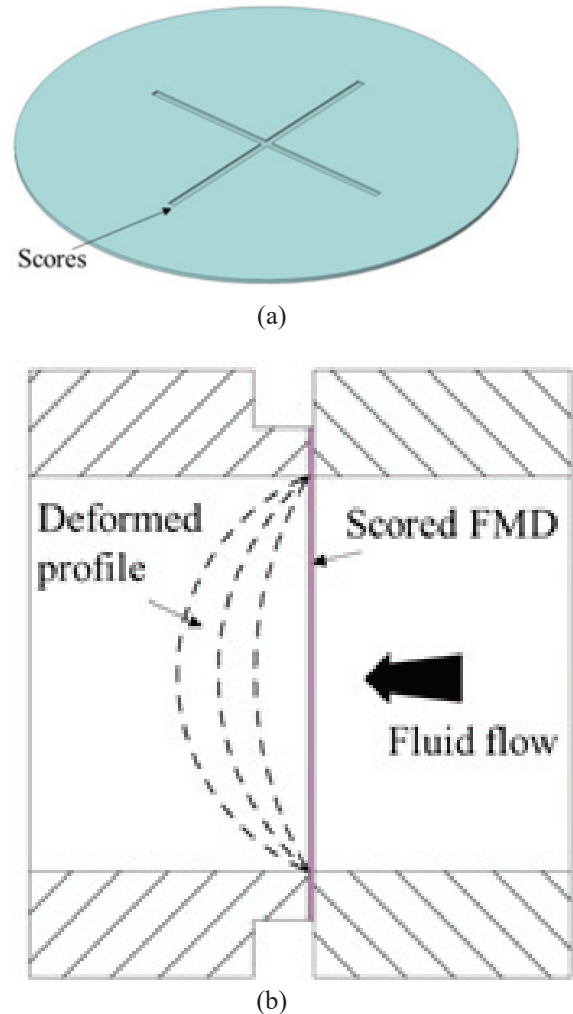

(a)

(b)

Figure 1. Flat metallic disc with scores: (a) Flat scored metallic disc (FSMD) and (b) FSMD in conditional burst application.

2. SIMULATION AND VALIDATION WITH EXPERIMENT

2.1 Geometry and Experimental Setup

2.1.1 Geometry

In order to establish the FEA methodology, the experimental work by Colombo et al.[20] on an FSMD is taken as the benchmark. This rupture disc is of 696 mm outer diameter with 2 mm thickness, as shown in Figure 2(a), and made of structural steel. The fluid exposed area, i.e., the pressure loading, is within a diameter of 481 mm. Two scores, i.e., grooves, are milled on one side of the disc in a cross configuration. The scores have 5 mm width and 0.80 mm deep and are located at 90° to each other, as seen in Fig. 2(b).

2.1.2 Experimental Setup

In the experimental setup[20], the disc is placed in a chamber and subjected to a quasi-static pressure loading on the plain, i.e., unscored side of the disc within 481 mm diameter, which is equal to the inlet pipe diameter. The pressure inside the chamber and strain gauge readings are monitored during the pressurisation process. Results from two strain gauges which are bonded on the scored side of the disc and away from scores location (as seen in Figure 2c where one is aligned with the *x*-axis and another along the *y*-axis) are taken for the purpose of comparing and validating the present FEA simulation.
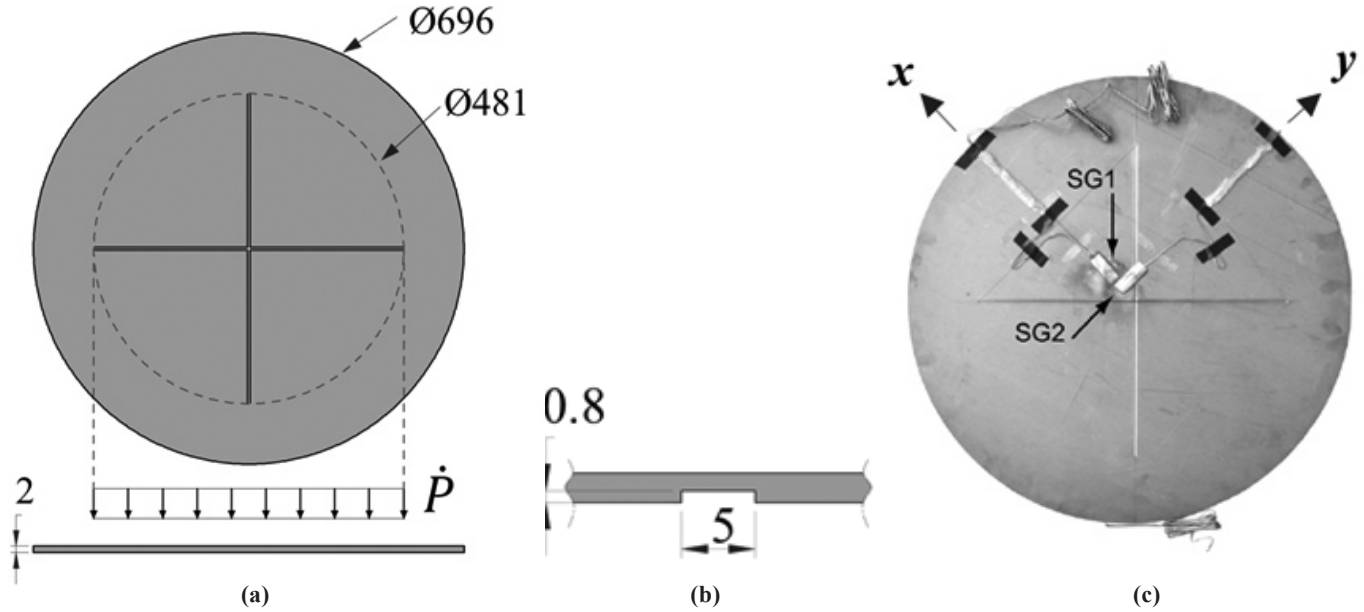
plastic strain, $\dot{\varepsilon}^* = \dot{\varepsilon}/\dot{\varepsilon}_0$ is the dimensionless normalised plastic strain rate considering the reference strain rate $\dot{\varepsilon}_0 = 1.0 s^{-1}$, $\dot{\varepsilon}$ is the strain rate, and $T^* = (T - T_{ref})/(T_m - T_{ref})$ is the homologous temperature of the material. A is the yield strength, n is the strain hardening exponent / constant, B is the strain hardening coefficient, C is the strain rate coefficient, m is the thermal softening parameter, T is the load-induced temperature rise in the material, and T_{ref} is the reference temperature. The first, second, and third terms in Eqn. (1) respectively capture the

Figure 2. Experimental disc geometry[20] (all dimensions in mm): (a) Geometry of flat SMD (b) Score geometry and (c) Strain gauge locations.

2.2 NUMERICAL SIMULATION

2.2.1 Material and Damage Models

The experimented metallic disc is made of S235 JR structural steel, and its mechanical properties are provided in Table 1. The material's constitutive behaviour is modelled with Johnson-Cook's (JC) strength model and its damage and failure with the Johnson-Cook damage model. These two models define the material's visco-plasticity and damage behaviour during loading in numerical simulation. These two models are capable of capturing the plasticity and damage in FSMD at low to high loading rates. The hydrostatic stress component of loading and associated pressure-volume relationship is captured through a linear equation of state.

Material Model

The flow stress-plastic strain relationship for metallic materials undergoing plastic deformation is best described by JC constitutive relation[22-23] which is given as

$$\sigma = \left[A + B\varepsilon^n\right]\left[1 + C\ln\dot{\varepsilon}^*\right]\left[1 - T^{*m}\right] \qquad (1)$$

where σ is the von-Mises flow stress, ε is the equivalent

large strain, strain rate, and thermal softening effects during loading. The material parameters of the JC constitutive model for the S235 JR structural steel considered in simulation have been taken from Zhong, *et al.*[24] and are given in Table 1.

Damage Model

The JC damage model is based on the fracture strain of the material[23,25]. The initiation and propagation of the damage in the material element is defined by

$$D = \sum \frac{\Delta\varepsilon}{\varepsilon^f} \qquad (2)$$

where $\Delta\varepsilon$ is the incremental plastic strain during the integration cycle and ε^f is the fracture strain which is given by the equation

$$\varepsilon^f = \left[D_1 + D_2 e^{D_3\sigma^*}\right]\left[1 + D_4\ln\dot{\varepsilon}^*\right]\left[1 + D_5 T^*\right] \qquad (3)$$

where $\sigma^* = \sigma_m/\overline{\sigma}$ is the dimensionless pressure, i.e., stress ratio, σ_m is the mean stress, $\overline{\sigma}$ is the von-Mises equivalent stress, and $D_1...D_5$ are the damage constants for the material, which can be determined from experiments.

The fracture or the element removal occurs when $D = 1$. The damage parameters for the S235 JR structural steel are not available in the literature. The damage parameters adopted in numerical simulations are mentioned in Table 1, which were finalised based on the iterative method with the initial values taken from Benerjee *et al.*[26]. All parameters were defined at a reference strain rate of $\dot{\varepsilon}^* = 0.0001 s^{-1}$.

Baker *et al.*[28] for the shock response of a blast loaded elastic oscillator was used to calculate the value of loading rate for the simulation, wherein for a quasi-static loading regime, the ratio of loading duration t_d with respect to the natural time period $(1/\omega_n)$ is given as

$$\omega_n t_d \geq 40 \tag{4}$$

Table 1. Elastic and material constants in JC material and damage models

	E (MPa)	μ	ρ (kg/m³)		
Elastic parameters	210000	0.3	7850		

	A (MPa)	B (MPa)	n	C	m
J-C material model (Initial values taken from Zhong *et al.*[24])	252	520	0.638	0.046	1.0

	D_1	D_2	D_3	D_4	D_5
J-C damage model (Initial values taken from Banerjee *et al.*[26])	0.05	0.8	0.44	-0.042	0

2.2.2 Model for FEA and Simulation Setup

The ABAQUS/Explicit[27] was adopted for creating the numerical model of the FSMD, as shown in Fig. 3 and its FEA simulation. Automatic time increment was adopted. The model was discretised with 583708 elements using the C3D8R element, which is an eight node brick element with reduced integration and hourglass control. All three degrees of freedom of nodes in the annular area of the disc between diameters 696 mm and 481 mm were fully constrained, as shown in Figure 3(b). Uniformly distributed pressure load was applied on the plain unscored side of the disc. Since the experiment was carried out at a quasi-static loading rate of 0.0132 MPa/s, to reach a burst pressure of the disc, i.e., $P_b = 1.15$ MPa, it took about 87.1 seconds to burst and rupture during experimentation. This experimental loading rate was too small for an explicit solver and needed to be accelerated in simulation to obtain an economic computation. Therefore, the approach provided in

The modal analysis of the thin FSMD shown in Fig. 2(a) resulted in the fundamental natural frequency ω_n as 82.29 Hz. Therefore, the Eqn. (4) results in $t_d = 0.486$ s. Considering the experimentally achieved maximum P_b of 1.15 MPa and the calculated t_d, the rate of loading rate was determined as 2.37 MPa/s and was adopted in the present numerical simulation.

2.2.3 Numerical Simulation

Mesh convergence studies were carried out to find the optimum number of elements through the thickness of the rupture disc. The number of elements through the thickness was increased in each iteration by keeping the same aspect ratio of elements in each model, i.e., the models were simulated with two, four, and six elements through the plate thickness. Burst pressure, burst time, central deflection, and maximum strain developed at the centre of the disc before the burst were studied during the mesh convergence analyses. The model with four
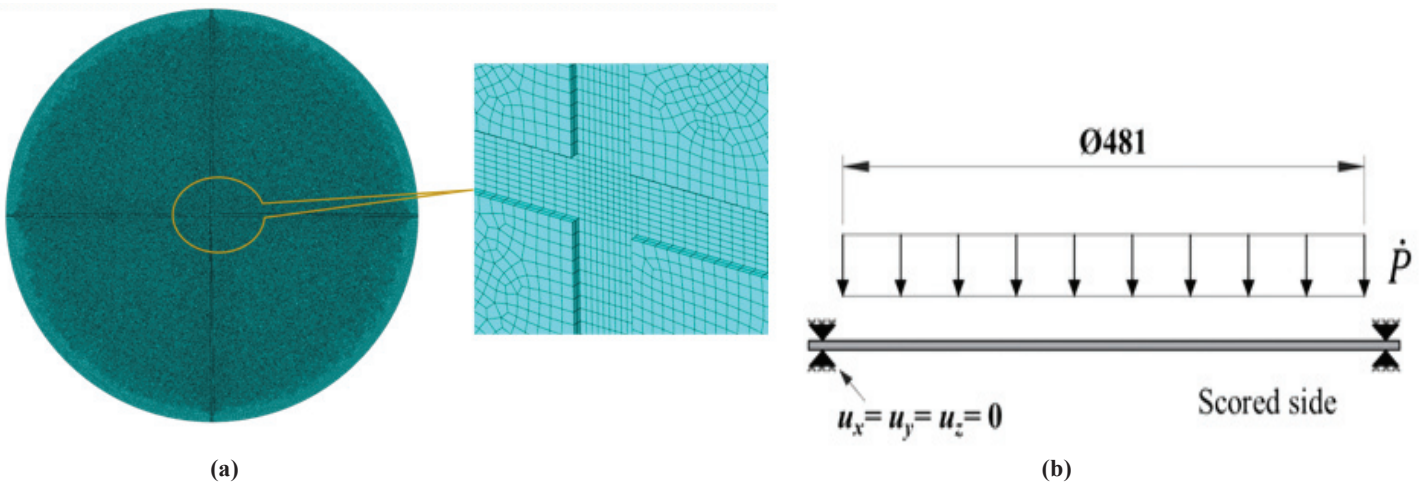

(a)   **(b)**

Figure 3. Simulation model: (a) FE model and (b) loads and boundary conditions.

elements through the plate thickness, i.e., 0.5 mm of element size, gave an economical and converged solution, which was considered for comparison and validation of FEA simulation with experimental results.

2.3 Simulation Results and Comparison with Experiments

The deformation pattern, applied pressure P, equivalent stress σ_{eq}, and equivalent strain ε_{eq} at different time instances, as viewed from scored side of the disc during loading, are shown in Fig. 4. At this small loading rate of 2.37 MPa/s, it is observed that the strain is concentrated along the score at the central region of the disc, as seen in Fig. 4(b). The failure is initiated at the score location away from the center of the disc at P = 0.98 MPa, as seen in Fig. 4(c). This failure is initiated when the accumulated plastic strain ε_{eq} reached the fracture strain ε^f as per the adopted JC's damage model, Eqn. (2). The failure is subsequently propagated towards the centre of the disc upon further loading, as observed in Figure 4(d). Comparison of P_b and the failure pattern between present simulation and experiment[20] is shown in Fig. 5, where predicted P_b is 0.98 MPa as against the experimentally reported average burst pressure of 1.01 MPa. The predicted P_b and the

failure pattern after the burst, as seen from the disc's scored side and the unscored side, matched reasonably well with the experimental results.

Normal strains are monitored at the two strain gauge locations, SG1 and SG2, as shown in Figure 2(c), where experimental results are reported. The predicted strains are compared with the experimental strain values in Figure 6(a-b). Although three discs experimented[20], the results of strains at the SG1 location in experiment-2 are only available, and the predicted strain profile matches very closely with that of the experiment, as seen in Figure 6(a). The results of strain at SG2 location from three experiments gave three different profiles *w.r.t.* the applied pressure as the bonded strain gauge SG2 would have experienced strain even after the occurrence of initial burst during subsequent deformation of the separated petals. The predicted strain at SG2 lies between the three experimental results, as seen in Fig. 6(b). Thus, the agreement of failure pattern, burst pressure, and strain profiles between the present simulation and experiment validate the adopted FEA simulation. Based on this validated numerical approach, the deformation and failure behaviour of the thin FSMD is investigated elaborately in the subsequent part of the paper.
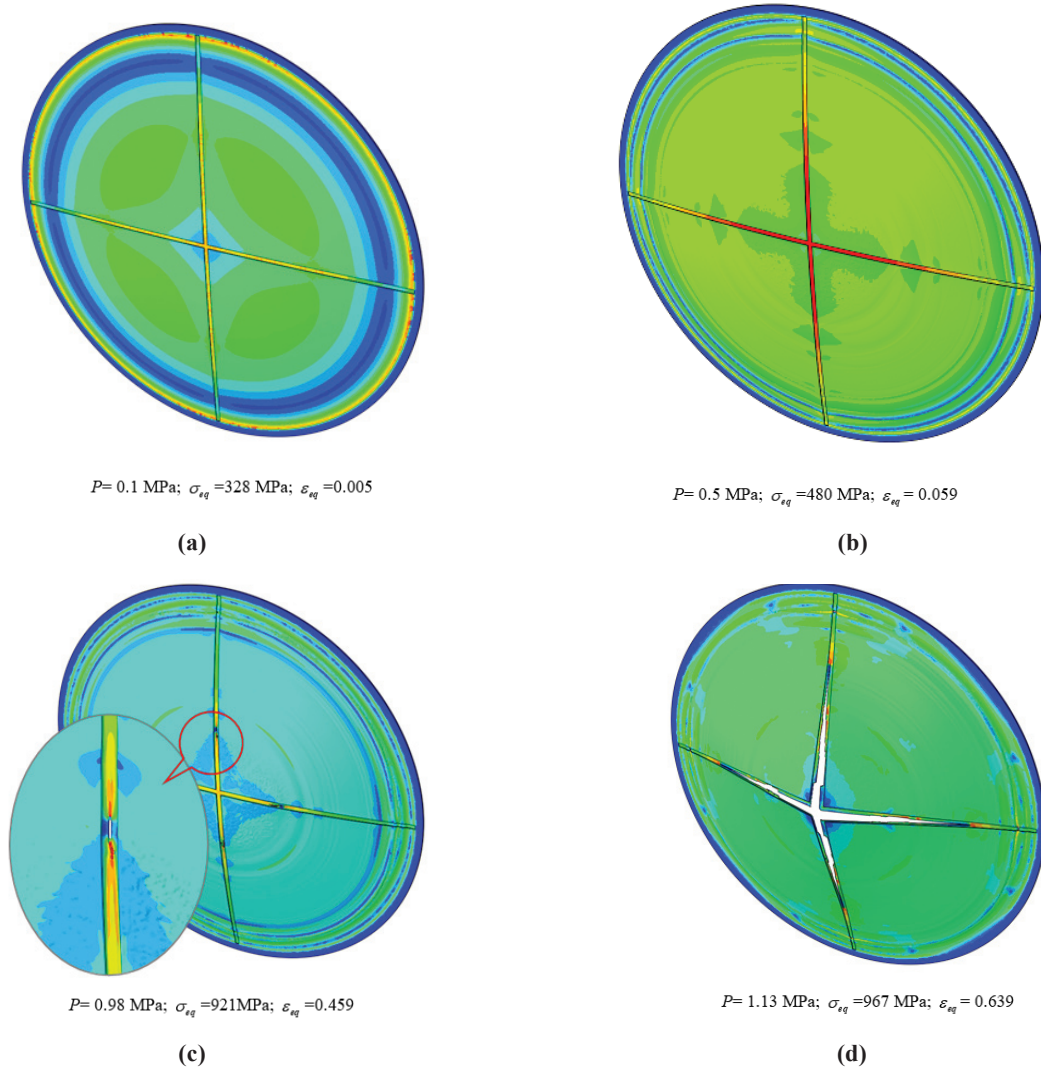

P= 0.1 MPa; σ_{eq} =328 MPa; ε_{eq} =0.005

(a)

P= 0.5 MPa; σ_{eq} =480 MPa; ε_{eq} = 0.059

(b)

P= 0.98 MPa; σ_{eq} =921MPa; ε_{eq} =0.459

(c)

P= 1.13 MPa; σ_{eq} =967 MPa; ε_{eq} = 0.639

(d)

Figure 4. Failure initiation and propagation: (a) At t = 43 ms (b) At t = 216 ms (c) At t = 416 ms and (d) At t = 478 ms.

3. RESPONSE TO VARIATIONS IN LOADING RATE AND GEOMETRICAL FEATURES

3.1 Effect of Loading Rate

In order to understand the effect of the increase in the loading rate on the failure behaviour of the FSMD, numerical studies are conducted at eight different loading rates such as 2.5, 5.0, 10, 25, 50, 100, 250 and 500 MPa/s. Five important responses such as P_b, burst time t_b, maximum central deflection w_{max}, maximum equivalent plastic strain ε_{max}, maximum
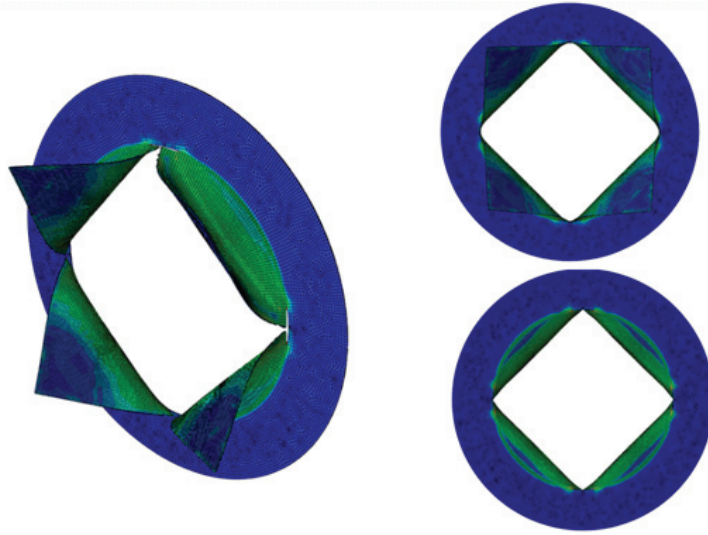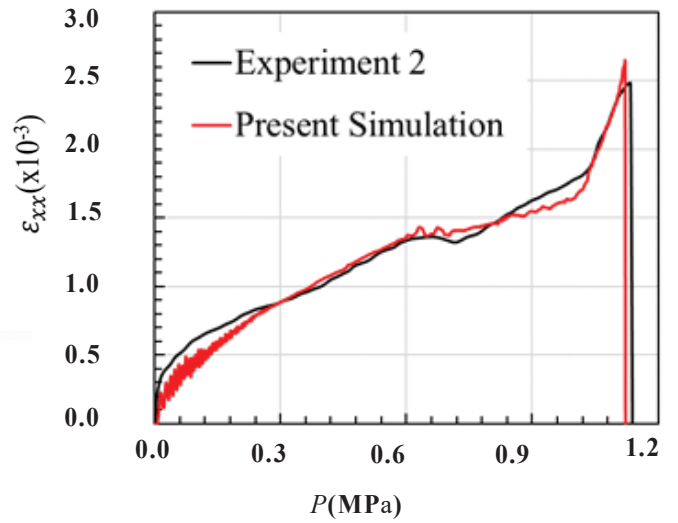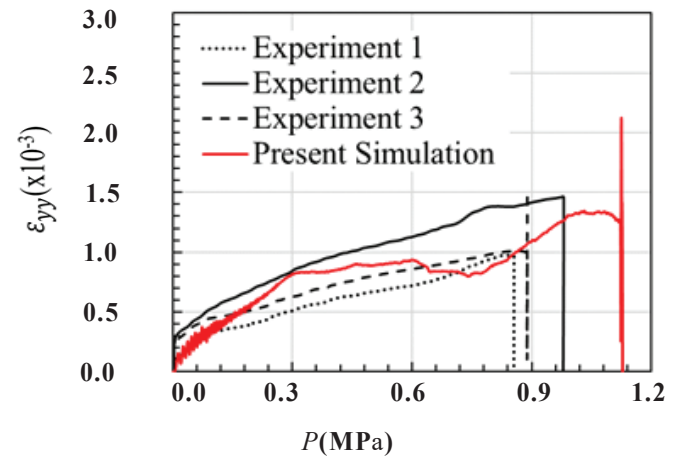
P_b = 0.98 MPa

(a)

P_b = 1.01 MPa

(b)

Figure 5. Comparison of deformed pattern, burst pressure and burst time between: (a) Present simulation and (b) Experiment.

(a)

(b)

Figure 6. Comparison of strains between present simulation and experiments at locations mentioned in Fig. 2(c): (a) Location-1 at SG-1 (45º from horizontal-left score) and (b) Location-2 at SG-2 (135º from horizontal-left score).

equivalent strain rate $\dot{\varepsilon}_{max}$ at the centre of the disc in score location just at a time step before the burst with an increase in applied pressure P are shown in Fig. 7(a). In this study, the geometry of the FSMD shown in Fig. 2 is considered. The P_b and w_{max} exhibit an increase, and t_b decrease when the loading rate increases from 2.5 to 100 MPa/s. Beyond 100 MPa/s, these responses exhibit significantly less sensitivity to loading rates and remain almost constant. On the other hand, ε_{max} increases steeply with the increase in loading rate up to 5.0 MPa/s. Afterwards, it almost remained insensitive to the loading rates from 5 to 100 MPa/s, beyond which it decreases gradually with the increase in loading rate. Unlike other responses, $\dot{\varepsilon}_{max}$ increases almost linearly with the increase in loading rate because of the increase in displacement rate of

the damaged element with the increase in loading rate. One peculiar observation is appreciable regarding the location of failure initiation *w.r.t.* the loading rates as showed in Fig. 7(b). When the loading rate varies from 2.5 to 25 MPa/s, the failure is initiated in the score location between 48 and 67 mm (i.e. at $r = 0.2R$-$0.28R$) away from the center. For loading rates > 50.0 MPa/s, the failure initiation occurs at center of the disc ($r = 0$) at the score location and is insensitive to the higher loading rates. This is because of the formation of plastic hinges along scores at locations away from the plate center under low loading rates and the corresponding increase in strain localisation. At high loading rates, more than 50 MPa/s, this phenomenon could not happen anywhere along the score except at the center of the plate.

3.2 Effect of Geometrical Features

The geometrical features in the FSMD significantly influence the deformation, failure and rupture behaviour when exposed to a given loading rate caused by fluid pressure. The influencing geometrical features can be i) diameter-to-plate (i.e. disc) thickness (D/t) ratio, ii) score depth-to-plate thickness (t_1/t) ratio, iii) score width-to-plate thickness (b/t) ratio, iv) score length-to-disc radius (l/R) ratio, v) score pattern i.e. the number of scores (N), and vi) score geometry. Numerical studies are conducted to investigate the effect of these geometrical features on the characteristics of FSMD, featured with four numbers of rectangular scores of width 5 mm and depth 0.8 mm as shown in Figure 2, under a pressure loading rate of 500 MPa/s. Only one geometrical feature to be investigated is varied in these sensitivity studies while maintaining the other features constant.

Consolidated list of various responses viz. P_b, t_b, w_{max}, ε_{max} and $\dot{\varepsilon}_{max}$ at the centre (i.e. at the intersection of scores) taken at the time of burst are presented in Table 2.

3.2.1 Diameter-to-Plate Thickness (d/t) Ratio

The effect of disc's diameter-to-plate thickness, i.e., D/t ratio, is investigated for six increasing diameters such as 50, 100, 250, 500, 750 and 1000 mm by keeping the plate thickness at $t = 2$ mm. The summary of all responses such as P_b, t_b, w_{max}, ε_{max} and $\dot{\varepsilon}_{max}$ with an increase in the D/t ratio is shown in Figure 7(c) and is also given in Table 2(a). It can be observed that both P_b and t_b decrease exponentially with an increase in D/t up to 250, and afterwards, their variations are very marginal. Variation of $\dot{\varepsilon}_{max}$ is bilinear with a shallow increase for D/t up to 250, followed by a steep increase thereafter. This is because of a considerable reduction in the plate stiffness beyond 500 mm diameter, accompanied by large displacement of the damaged element. The ε_{max} exhibit less sensitivity to variation in D/t and remains almost insensitive for $D/t \leq 50$ and decreases from 0.44 to 0.30 for $50 \leq D/t \leq 500$. With the increase in D/t from 25-50, maximum mid-deflection increases almost linearly from 10 mm to 65 mm due to a consistent decrease in the plate stiffness.

3.2.2 Score Length-to-Disc Radius (l/R) Ratio

The effect of the score's length-to-disc radius (i.e. *l/R*) ratio is investigated by varying the score's length from 48mm

to 240.5mm for a constant disc radius of 240.5 mm to achieve *l/R* ratios of 0.2, 0.4, 0.5, 0.6, 0.8 and 1.0. Other geometric parameters of disc and score are kept constant.

The behaviour of the FSMD for the analysed *l/R* variations is shown in Figure 7(d), and a summary of maximum values of responses are given in Table 2(a). It is seen that P_b, t_b and w_{max} decrease gradually for *l/R* up to 0.4, beyond which these responses remain constant. The ε_{max} is very much insensitive to variations in *l/R*. The $\dot{\varepsilon}_{max}$ increases from 0.6s^{-1} to 0.9s^{-1} for $0.2 \leq l/R \leq 0.4$, and afterwards, it remains unchanged with any further increase in *l/R*. This study reveals that the responses in FSMD are sensitive only for the score's length up to 50% of the disc radius. By and large, they are relatively insensitive to any variations in the *l/R* ratio.
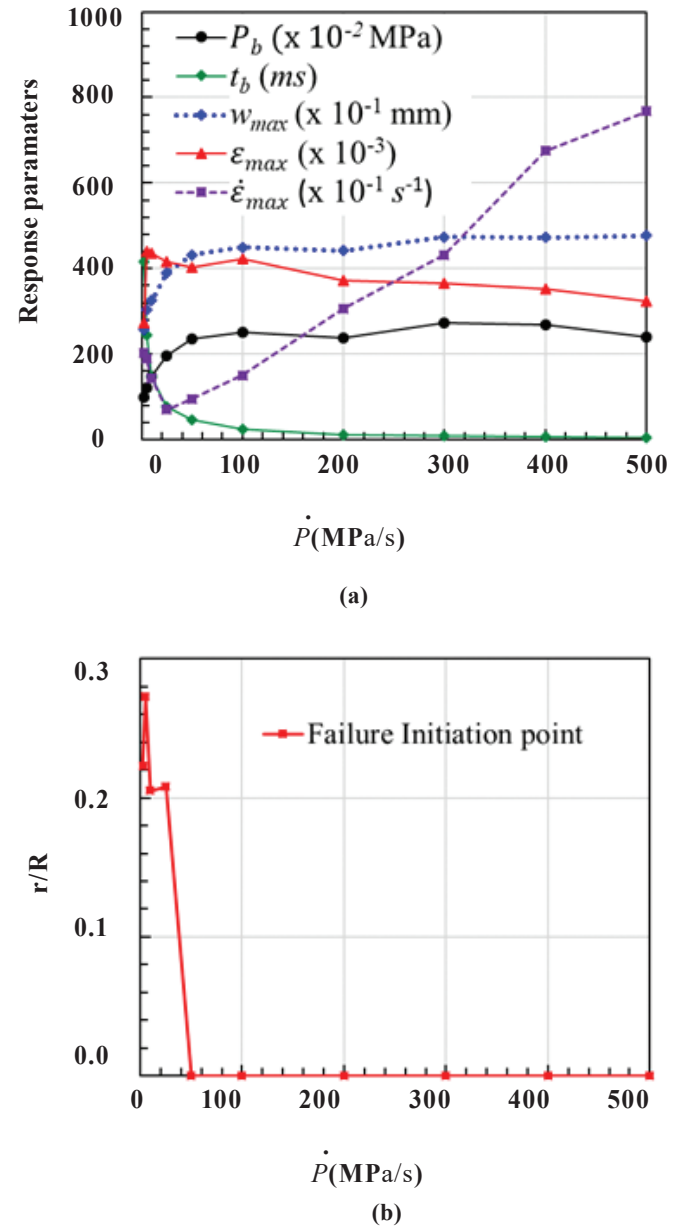
(a)

(b)

Figure 7. Response of FSMD under the influence of loading rate and different geometric parameters: (a) Loading rate (b) Failure initiation w.r.t. loading rate.

(c)
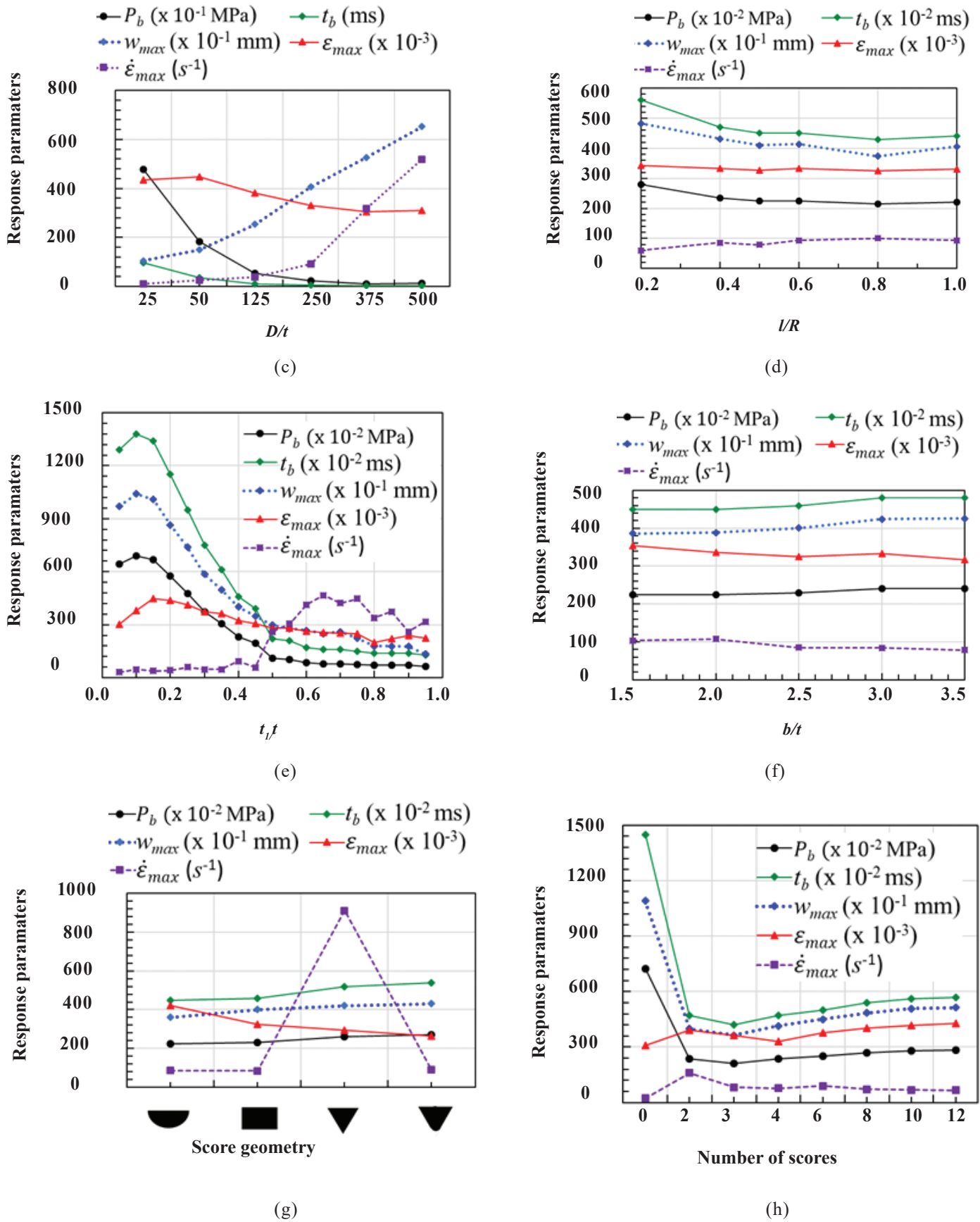

(d)

(e)

(f)

(g)

(h)

Figure 7. Response of FSMD under the influence of loading rate and different geometric parameters: (c) Plate diameter to plate thickness ratio (d) Score's length to max. disc radius (e) Score's depth to plate thickness ratio (f) Score's width to plate thickness ratio (g) Score's geometry and (h) Number of scores.

3.2.3 Score's Depth-to-Plate Thickness (t_1/t) Ratio

The effect of score depth t_1 is analysed by varying t_1 from 0.1 mm to 1.9 mm in steps of 0.1 mm by keeping constant values for the plate thickness ($t = 2$ mm) and score's width ($b = 5$ mm). This variation of score's depth provides $0.05 \leq t_1/t \leq 0.95$ in steps of 0.05. The effect of t_1/t on responses of the FSMD is shown in Fig. 7(e), and their maximum values are given in Table 2(b). It can be observed that P_b, t_b and w_{max} increase with an increase in t_1/t up to 0.1 and afterwards, they decrease almost asymptotically with the increase in t_1/t up to 0.5. For $t_1/t \geq 0.5$, both P_b and t_b remain constant while w_{max} decrease linearly with a shallow slope. Variation in $\dot{\varepsilon}_{max}$ is insignificant for any increase in t_1/t up to 0.45, it increases from 60 s^{-1} to 450 s^{-1} for $0.45 \leq t_1/t \leq 0.65$, and it decreases gradually from 450 s^{-1} to 300 s^{-1} for $0.65 \leq t_1/t \leq 0.95$. On the other hand, ε_{max} increases with the increase in t_1/t up to 0.15. It decreases gradually from 0.45 to 0.25 for $0.15 \leq t_1/t \leq 0.95$. This study reveals that all the important response parameters exhibit almost insensitivity for a score depth more than $0.6t$.

3.2.4 Score's Width-to-Plate Thickness (b/t) Ratio

The influence of score's width b is analysed by varying the score's width from 3.0 mm to 7.0 mm in steps of 1.0 mm by keeping constant values for the disc thickness $t = 2$ mm and score's depth $t_1 = 0.8$ mm. This variation of score's width provides a width-to-plate thickness ratio as $b/t = 1.5, 2.0, 2.5, 3.0$ and 3.5. The behaviour of the FSMD is shown in Figure 7(f). It can be observed that all response parameters remain almost constant except little variation for any increase in b/t ratio from 1.5 to 3.5. Only a small variation of about 2 MPa in P_b, 0.3 ms in t_b, 3 mm in w_{max}, 0.03 in ε_{max} and about 20s^{-1} in $\dot{\varepsilon}_{max}$ are observed with the considered variation in b/t ratio. This study demonstrates that the score's b/t ratio does not significantly influence the important response parameters in the FSMD.

3.2.5 Score Geometry

In all the previous studies thus discussed, a rectangular score geometry was considered. The score geometry can be semi-circular, rectangular, triangular and triangular with tip fillet in cross-sections. Their influence on the deformation and rupture in the FSMD is investigated by keeping constant dimensions for the plate thickness $t = 2.0$ mm, score's width $b = 5.0$ mm, and score's depth $t_1 = 0.8$ mm. The maximum values of all responses such as P_b, t_b, w_{max}, ε_{max} and $\dot{\varepsilon}_{max}$ for all four score geometries are shown in Figure 7(g) and also given in Table 2(b). All response parameters are almost identical for the semi-circular and rectangular score geometries. Triangular and tip-filleted triangular score geometries exhibit marginally higher responses. Except for a higher value of $\dot{\varepsilon}_{max}$ for the triangular score geometry, which may be attributed to the sharp stress concentration effect on the triangular score tip, all the other response parameters are almost the same for the four score cross-sections studied. Based on this study, the score geometry with rectangular cross-section is preferable considering the manufacturing easiness and dimensional control. The next recommendable geometry is the tip-filleted triangular score which can be made by press tools.

3.2.6 Score Pattern, i.e., the Number of Scores (N)

Scores provided in the disc act as regions of local stress concentration in the FSMD. The effect of the number of scores on the FSMD is studied by varying the number of scores N from 0 to 12, i.e., at $N = 0, 2, 3, 4, 6, 8, 10$ and 12. During this variation, the plate thickness $t = 2$ mm, score's width $b = 5$ mm, and score's depth $t_1 = 0.8$ mm are maintained constant. Introduction of 2 scores along the diagonal of the disc reduced the responses such as P_b, t_b, w_{max} and ε_{max} significantly as compared to an unscored flat metallic disc, as shown in Figure 7(h). These responses are very minimal for $N = 3$, and for $N > 3$, their increase is very gradual, and after $N > 8$, the responses are almost constant. The $\dot{\varepsilon}_{max}$ is insensitive to an increase in $N > 3$.

Failure propagation and failure pattern entirely depend on the pressure acting on petals after the initial burst. However, for this analysis, the pressure is assumed to be acting continuously on the disc throughout the simulation, which is causing failure propagation and petal separation. The predicted failure patterns just after the burst with N ranging from 0 to 12 are shown in Fig. 8. The strain rate is relatively higher in FSMD with $N = 2$ as compared to discs with the higher number of scores, as
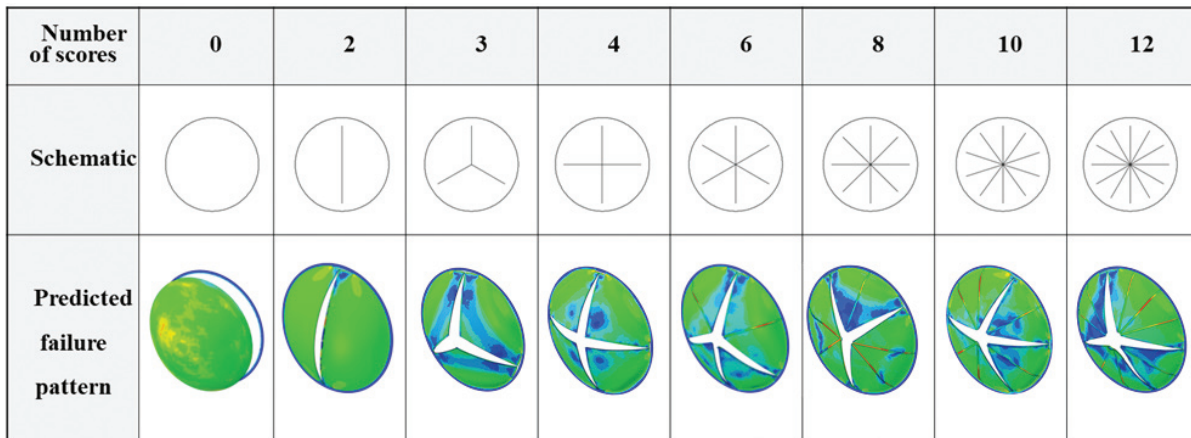

Figure 8. Predicted failure pattern without and with number of scores in the disc.

481

Table 2(a). Influence of geometrical features on the response of flat SMD

	D/t					l/R					Number of scores							
	25	50	125	250	500	0.2	0.4	0.6	0.8	1.0	0	2	3	4	6	8	10	12
P_b (MPa)	47.7	18.3	5.3	2.2	1.15	2.80	2.35	2.25	2.15	2.20	7.25	2.35	2.10	2.35	2.50	2.70	2.80	2.85
t_b (ms)	95.4	36.6	10.6	4.4	2.3	5.6	4.7	4.5	4.3	4.4	14.5	4.7	4.2	4.7	5.0	5.4	5.6	5.7
w_{max} (mm)	10.5	14.9	25.3	40.5	65.2	48.3	43.1	41.4	37.4	40.6	109	39.8	36.3	41.4	45.0	48.4	50.8	51.3
ε_{max}	0.43	0.45	0.38	0.33	0.31	0.34	0.33	0.33	0.33	0.33	0.31	0.39	0.36	0.33	0.38	0.40	0.42	0.43
$\dot{\varepsilon}_{max}$ (s^{-1})	9	24	39	91	519	60	86	94	100	93	23	160	83	77	90	72	69	67

Table 2(b). Influence of geometrical features on the response of flat SMD

	t_l/t					b/t					Geometry			
	0.05	0.25	0.5	0.75	0.95	1.5	2	2.5	3	3.5	◖	▬	▼	▼
P_b (MPa)	6.5	4.8	1.1	0.75	0.65	2.25	2.25	2.30	2.40	2.40	2.25	2.30	2.60	2.70
t_b (ms)	12.9	9.5	2.2	1.5	1.3	4.5	4.5	4.6	4.8	4.8	4.5	4.6	5.2	5.4
w_{max} (mm)	97.1	73.9	29.9	22.3	13.4	38.5	38.8	40.1	42.4	42.5	36.0	40.1	42.1	43.2
ε_{max}	0.30	0.41	0.28	0.25	0.23	0.35	0.34	0.32	0.33	0.32	0.42	0.32	0.29	0.26
$\dot{\varepsilon}_{max}$ (s^{-1})	32	61	261	448	318	103	108	85	84	78	86	85	911	89

seen in Table 2(a) and Fig. 7(h). This is because the petals are formed after the burst along the two scores, and they are forced to undergo tearing at the fixed boundary before the petals experience bending under the effect of increasing fluid pressure. This tearing at the petal ends results in large displacements, i.e., strain in a given time increment and therefore leading to a large strain rate. Clear petal separation is observed for all FSMD along the scores with $N = 3$ to 4, and they can bend freely at the fixed boundary after the petal formation upon the increase in fluid pressure. For $N > 4$, the failure is observed only along few scores, which reveals that, as the N increases, the failure may not be initiated and propagated along all the scores as seen in Figure 8 because only a few scores experienced the failure limits and underwent petal separation along these scores and the remaining scores in between the separated scores did not reach the failure limits and remained intact without any separation. This can also be triggered by non-uniformities in dimensional tolerances in the score cross-sections. This reveals that the minimum number of scores that can be recommended to be employed in FSMD can be 3 or 4 to achieve a clear separation and subsequent bending along the fixed boundary.

4. CONCLUSIONS

The large deformation and failure behaviour of a thin flat scored metallic disc subjected to an impulsive pressure loading has been investigated. The predicted plastic strains, burst pressure and deformation pattern agreed well with the experimental results for the reference case. The behaviour of an FSMD under the effect of loading rates (2.5-500 MPa/s), diameter-to-plate thickness ratio (50-500), score's depth-to-plate thickness ratio (0.05-0.95), score's width-to-plate thickness ratio (1.5-3.5), score's length-to-disc radius ratio (0.2-1.0), score pattern (with the number of scores from 0-12), and score geometry (semi-circular, rectangular, triangular and triangular with filleted tip) were thoroughly investigated. The following important conclusions can be drawn from this paper.

- Scores provided on the thin flat metallic disc ensure the failure initiation and propagation along them.
- Burst pressure, burst time and central deflection are almost constant to loading rates beyond 100 MPa/s.
- At loading rates ≤ 25 MPa/s, the failure is initiated in score between $r/R = 0.20$-0.28 and propagated towards the disc centre and fixed boundary, whereas at all higher loading rates, the failure is always initiated at $r/R = 0$ and propagated towards the fixed boundary.
- Required P_b and t_b can be chosen in FSMD when $D/t < 250$, beyond which the responses are unaffected.
- All response parameters are sensitive to variation in score's depth only up to 60% of the plate thickness.
- The behaviour of FSMD is insensitive to any changes in the score's width, i.e., b/t ratio.
- FSMD with desired response parameters can be achieved only when the length of the score is less than 40% of the disc radius, as all response parameters achieve a stabilised value for $l/R > 0.4$.
- Responses are very minimal for the number of scores $N = 3$. Responses remained almost constant for $N > 8$. There is no clear separation of petals along all the scores for $N > 4$.
- The P_b and t_b are almost insensitive for all the four score geometries. Responses are almost the same for the semi-circular and rectangular score geometries. Rectangular geometries offer manufacturing easiness and dimensional control. Hence, they can be recommended choices.

REFERENCES

1. Smith, P. & Zappe, R.W. 6-Rupture Discs: Valve Selection Handbook (5th Edition), Gulf Professional Publishing, 2004, 227–267.
   doi:10.1016/B978-075067717-2/50006-7

2. Aune, V.; Fagerholt, E.; Langseth, M. & Børvik, T. A shock tube facility to generate blast loading on structures. *Int. J. Prot. Struct.*, 2016, **7**(3), 340–366. doi:10.1177/2041419616666236

3. Nurick, G.N. & Martin, J.B. Deformation of thin plates subjected to impulsive loading-A review: Part I: Theoretical considerations. *Int. J. Impact. Eng.*, 1989, **8**(2), 159–170.
   doi:10.1016/0734-743X(89)90014-6

4. Nurick, G.N. & Martin, J.B. Deformation of thin plates subjected to impulsive loading-a review Part II: Experimental studies. *Int. J. Impact. Eng.*, 1989, **8**(2), 171-186.
   doi:10.1016/0734-743X(89)90015-8

5. Yuen, S.C.K.; Nurick, G.N.; Langdon, G.S. & Iyer, Y. Deformation of thin plates subjected to impulsive load: Part III - an update 25 years on. *Int. J. Impact. Eng.*, 2017, **107**, 108–117.
   doi:10.1016/j.ijimpeng.2016.06.010

6. Nurick, G.N. & Shave, G.C. The deformation and tearing of thin square plates subjected to impulsive loads – An experimental study. *Int. J. Impact. Eng.*, 1996, **18**(1), 99-116.
   doi:10.1016/0734-743X(95)00018-2

7. Olson, M.D. Efficient modelling of blast loaded stiffened plate and cylindrical shell structures. *Int. J. Comp. & Struct.*, 1991, **40**(5), 1139-1149.
   doi:10.1016/0045-7949(91)90385-Y

8. Smith, R.G.T & Nurick, G.N. The deformation and tearing of thin circular plates subjected to impulsive loads. *Int. J. Impact. Eng.*, 1991, **11**(1), 77–91.
   doi:10.1016/0734-743X(91)90032-B

9. Nurick, G.N.; Gelman, M.E. & Marshall, N.S. Tearing of blast loaded plates with clamped boundary conditions. *Int. J. of Impact. Eng.*, 1996, **18**(7-8), 803-827. doi:10.1016/S0734-743X(96)00026-7

10. Bonorchis, D. & Nurick, G.N. The effect of welded boundaries on the response of rectangular hot-rolled mild steel plates subjected to localised blast loading. *Int. J. Impact. Eng.*, 2007, **34**(11), 1729-1738.
    doi:10.1016/j.ijimpeng.2006.11.002

11. Gupta, N.K. & Nagesh. Deformation and tearing of circular plates with varying support conditions under uniform impulsive loads. *Int. J. Impact. Eng.*, 2007, **34**(1), 42–59.
    doi:10.1016/j.ijimpeng.2006.05.002

12. Jacob, N.; Nurick, G.N. & Langdon, G.S. The effect of stand-off distance on the failure of fully clamped circular mild steel plates subjected to blast loads. *Eng. Struct.* 2007, **29**(10), 2723–2736.
    doi:10.1016/j.engstruct.2007.01.021

13. Goel, M.D.; Matsagar, V.A. & Gupta, A.K. Dynamic response of stiffened plates under air blast. *Int. J. of Prot. Struct.*, 2011, **2**(1), 139–155.
    doi:10.1260/2041-4196.2.1.139

14. Nagesh. & Gupta, N.K. Large deformations and tearing of circular plates and plate-tube structural combinations under impulsive loading. *Procedia Eng.*, 2017, **173**, 526-532.
    doi:10.1016/j.proeng.2016.12.083

15. Nurick, G.N.; Olson, M.D.; Fagnan, J.R. & Levin, A. Deformation and tearing of blast-loaded stiffened square plates. *Int. J. Impact. Eng.*, 1995, **16**(2), 273-291.
    doi:10.1016/0734-743X(94)00046-Y

16. Yuan, Y. & Tan, P.J. Deformation and failure of rectangular plates subjected to impulsive loadings. *Int. J. Impact. Eng.*, 2013, **59**, 46–59.
    doi:10.1016/j.ijimpeng.2013.03.009

17. Rudrapatna, N.S.; Vaziri, R. & Olson, M.D. Deformation and failure of blast-loaded square plates. *Int. J. Impact. Eng.*, 1999, **22**(4), 449-467.
    doi:10.1016/S0734-743X(98)00046-3

18. Smith, R.G.T. & Nurick, G.N. The deformation and tearing of thin circular plates subjected to impulsive loads. *Int. J. Impact. Eng.*, 1991, **11**(1), 77-91.
    doi:10.1016/0734-743X(91)90032-B

19. Jeong, J.Y.; Jo, W.; Kim, H.; Baek, S.H. & Lee, S.B. Structural analysis on the superficial grooving stainless-steel thin-plate rupture discs. *Int. J. Precis. Eng. Manuf.*, 2014, **15**, 1035–1040.
    doi:10.1007/s12541-014-0433-7

20. Colombo, M.; Martinelli, P. & Prisco, M.D. Validation of a computational approach to predict bursting pressure of scored steel plates. *Exp. Mech.* 2014, **54**, 1555–1573.
    doi:10.1007/s11340-014-9916-9

21. ASME BPVC-VII-1-2017. BPVC Section VIII-Rules for Construction of Pressure Vessels Division 1, ASME 2017.

22. Johnson, G.R. & Cook, W.H. A constitutive model and data from metals subjected to large strains, high strain rates and high temperatures. *In* Proc. 7th Int. Symp. on Ballistics, Hague, Netherlands, 1983, 541–547.

23. Rao, C.L.; Narayanamurthy, V. & Simha, K.R.Y. Applied Impact Mechanics. Wiley 2016.
    doi:10.1002/9781119241829

24. Zhong, W.Z.; Mbarek, I.A.; Rusinek, A.; Bernier, R.; Jankowiak, T. & Sutter, G. Development of an experimental set-up for dynamic force measurements during impact and perforation, coupling to numerical simulations. *Int. J. Impact. Eng.*, 2016, **91**, 102–115.
    doi:10.1016/j.ijimpeng.2016.01.006

25. Johnson, G.R. & Cook, W.H. Fracture characteristics of three metals subjected to various strains, strain rates, temperatures and pressures. *Eng. Fract. Mech.*, 1985, **21**(1), 31–48.
    doi:10.1016/0013-7944(85)90052-9

26. Banerjee, A,; Dhar, S.; Acharyya, S.; Datta, D. & Nayak, N. Determination of Johnson cook material and failure model constants and numerical modelling of Charpy impact test of armour steel. *Mat. Sci. Eng. – A*, 2015,

640, 200–209. doi:10.1016/j.msea.2015.05.073

27. ABAQUS/Explicit User's manual, V6.6. Dassault Systèmes Simulia Corporation, France, 2006.

28. Baker, W.E.; Cox, P.A.; Westine, P.S.; Kulesz, J.J. & Strehlow, R.A. Structural Response: Simplified Analysis Techniques. Fundamental Studies in Engineering, Explosion Hazards and Evaluation. *Elsevier Sci.,* 1983, **5**, 273-364.
   doi: 10.1016/B978-0-444-42094-7.50012-4.

CONTRIBUTORS

Mr Kanakadandi Gopinath has completed BTech Mechanical Engineering from Jawaharlal Nehru Technological University, Hyderabad and working as Scientist D at Research Centre Imarat, Hyderabad.
He has carried out the research activity on investigating the response of thin flat scored metallic disc subjected to impulsive loadings.

Dr Vijayabaskar Narayanamurthy is currently working as Scientist F at Research Centre Imarat, Hyderabad.
He has primarily guided the research, methodology and nonlinear FEA.

Dr Venkata Daseswara Rao Yendluri has a PhD in mechanical engineering from NIT, Raipur.
He has mentored the research work and formulation of the problem.